Open your mind. LUT.
Lappeenranta University of Technology

Modeling and PID-Control Design for Bearingless High Speed Motor Drive

Anton Mussalo

Simo Janhunen

Bachelor's Thesis
LUT School of Energy Systems
Electrical Engineering

28.9.2018

ABSTRACT

Lappeenranta University of Technology
LUT School of Energy Systems
Electrical Engineering

Anton Mussalo and Simo Janhunen
Modeling and PID-Control Design for Bearingless High Speed Motor Drive
2018

Bachelor's Thesis
38 pages, 27 figures, 2 tables, 1 appendix
Examiners: D.Sc. (Tech.) Niko Nevaranta, M.Sc. Pekko Jaatinen
Keywords: bearingless machine, magnetic bearing, modeling, simulation, PID tuning

The demand for higher rotational speeds and the more and more challenging work environments have pushed magnetic bearings and bearingless machines to be an extensive multidisciplinary field of research. Magnetic bearings are used to support ferromagnetic objects using magnetic levitation in a way that there is no mechanical contact between the rotating part and the magnetic bearing. The contactless principle makes magnetic bearings useful in applications like turbomolecular pumps and high speed motors. In bearingless machines, the function of a magnetic bearing is integrated into an electric motor to create a bearingless unit that generates both the forces needed for magnetic levitation as well as the torque.

In this study, a simulation model for a magnetic bearing system with four degrees of freedom (4-DOF) is created and a PID-based position controller is implemented. The model is used to illustrate the position control in a bearingless machine. A controller solution is proposed and later simulated. Finally, the control system is tested on the actual prototype machine.

The simulation model shared similar behavior when compared to the prototype machine, thus concluding the validity of the model. Based on the experimental results, the proposed controller worked adequately gaining a stable lift-up and having moderate responses to slight displacements. A minor oscillation was found that requires further study.

TIIVISTELMÄ

Lappeenrannan teknillinen yliopisto
LUT School of Energy Systems
Sähkötekniikka

Anton Mussalo ja Simo Janhunen
Modeling and PID-Control Design for Bearingless High Speed Motor Drive
2018

Kandidaatintyö
38 sivua, 27 kuvaa, 2 taulukkoa, 1 liitettä
Tarkastajat: TkT Niko Nevaranta, DI Pekko Jaatinen
Hakusanat: bearingless-kone, magneettilaakeri, mallintaminen, simulointi, PID-säätö

Vaatimukset suuremmista pyörimisnopeuksista ja yhä haastavammat käyttöympäristöt ovat tehneet magneettilaakereista ja bearingless-koneista laajan monitieteellisen tutkimuskohteen. Magneettilaakereita käytetään leijuttamaan ferromagneettisia kappaleita magneettikentällä ilman laakerin ja kappaleen välistä fyysistä kontaktia. Kosketukseton toimintaperiaate tekee bearingless-koneista käyttökelpoisia sovelluksissa kuten turbomolekulaariset pumput sekä suurnopeusmoottorit. Bearingless-koneissa magneettilaakerin toiminta on integroitu sähkömoottoriin, jolloin moottori tuottaa väännön lisäksi myös leijutukseen tarvittavat magneettiset voimat.

Tässä työssä luodaan simulaatiomalli neljän vapausasteen magneettilaakerisysteemille, jolle suunnitellaan paikkasäätö käyttäen PID-säädintä. Tätä mallia ja säädintä voidaan hyödyntää testilaitteena toimivassa bearingless-koneessa. Säädinratkaisu esitetään ja simuloidaan. Lopuksi suunniteltu säätöjärjestelmä testataan prototyyppikoneella.

Simulaatiomalli vastasi käyttäytymiseltään prototyyppilaitetta vahvistaen mallin oikeellisuuden. Mittausten avulla todettiin simulointimallin oikeellisuus. Tuloksien perusteella ehdotettu säädin toimi riittävän hyvin saaden stabiilin nousun sekä kohtalaiset vasteet pienille siirtymille. Löydettiin pieni oskillaatio, joka vaatii syvällisempää tarkastelua.

Table of Contents

SYMBOLS AND ABBREVIATIONS

Symbols

A	projected area
$\boldsymbol{A}$	system matrix
A_{a}	cross-sectional area of air
A_{fe}	cross-sectional area of iron
a	distance from bearing A to center
$\boldsymbol{B}$	input matrix
B	magnetic flux density
b	distance from bearing B to center
$\boldsymbol{C}$	output matrix
$C(s)$	controller
$C_D(\mathrm{s})$	controller's derivate component
$\boldsymbol{D}$	feedforward matrix
e	position error
e_{ss}	steady state error
$\boldsymbol{F}_{\mathrm{b}}$	bearing force vector
$\boldsymbol{F}_{\mathrm{g}}$	gravitational force vector
f_{+}	force in the positive direction
f_{-}	force in the negative direction
f	force
f_{g}, G	gravitational pull
f_{m}	magnetic pull
f_{x}	force vector in x-axis
$f_{\mathrm{xA}}, f_{\mathrm{xB}}$	bearing force in x-axis
f_{y}	force vector in y-axis
$f_{\mathrm{yA}}, f_{\mathrm{yB}}$	bearing force in y-axis
g	acceleration of gravity
i'	current in coil
i_0	bias current
i_{c}	control current
$\boldsymbol{i}_{\mathrm{c}}$	control current vector

$\boldsymbol{i}_{\mathrm{cg}}$	compensation current
$i_{\mathrm{c,x}}$	control current in x-axis (2-DOF)
$i_{\mathrm{c,xA}}$, $i_{\mathrm{c,xB}}$	control current in x-axis (4-DOF)
$i_{\mathrm{c,y}}$	control current in y-axis (2-DOF)
$i_{\mathrm{c,yA}}$, $i_{\mathrm{c,yB}}$	control current in y-axis (4-DOF)
i_{s}	current spike
J	inertia
$\mathbf{K}_{\mathrm{i}}$	current stiffness matrix
k_{i}	current stiffness
$\mathbf{K}_{\mathrm{s}}$	position stiffness matrix
k_{s}	position stiffness
K_{p}	proportional gain
K_{i}	integral gain
K_{d}	derivative gain
$\mathbf{M}_{\mathrm{b}}$	mass matrix of the rotor
$\mathbf{M}_{\mathrm{c}}$	mass matrix of the rotor regarding its center of mass
m	mass
N	number of turns in coil
N_{x}	moment around x-axis
N_{y}	moment around y-axis
r	measured feedback
s	Laplace variable
$\mathbf{T}$	transformation matrix
T_{d}	derivate time
T_{f}	filter parameter
u	voltage
$\boldsymbol{u}$	input vector
$\boldsymbol{x}$	state vector
x, x_{A}, x_{B}	position in x-axis
x'	displacement in x-axis
x_0	air gap in equilibrium state
x_{ref}	reference value for position
$\boldsymbol{y}$	output vector

$y_{\mathrm{A}}, y_{\mathrm{B}}$	position in y-axis
$\boldsymbol{z}_{\mathrm{b}}$	position vector
$\ddot{\boldsymbol{z}}_{\mathrm{b}}$	acceleration vector
α	angle of magnetic pull
θ_{x}	angular position of x
θ_y	angular position of y
μ_0	permeability in vacuum
μ_{r}	permeability in substance
ξ	damping coefficient
ω	frequency
ω_{n}	natural frequency

Abbreviations

AMBs	active magnetic bearings
DOF	degrees of freedom
HMBs	hybrid magnetic bearings
MIMO	multiple-input multiple-output
PD	proportional-derivate
PID	proportional-integral-derivate
PIDf	proportional-integral-derivate-filter
PMBs	passive magnetic bearings
SISO	single-input single-output

1 INTRODUCTION

Magnetic bearings enables the suspension of ferromagnetic objects, such as rotors, without having any physical contact by using magnetic fields. As there is no mechanical contact there is no wear and therefore lubrication is not required (Kurvinen, 2016). Traditional mechanical bearings show disadvantages when compared to magnetic bearings, like friction, susceptibility to damage from impurities in lubrication system, lower revolutions per minute capacity and lower vibration damping. These drawbacks limit their usability in high speed technology. (Gieras, 2010; Adamczak, et al., 2017) Therefore, magnetic bearings are widely used in high speed applications and especially in processes with challenging environmental conditions e.g., food industry. Additionally, systems mounted with magnetic bearings can be utilized in vacuums and extreme temperatures, where traditional types of bearings cannot function properly. (Schweitzer, et al., 2009; Lantto, 1999)

Magnetic pull in active magnetic bearings is formed by electromagnets; strength of the magnetic pull is controlled by the current that is fed to its actuator's coils. The magnetic pull in passive magnetic bearings is formed by permanent magnets; the ferromagnetic material and its dimensions determine the strength of the magnetic pull or repel. In order to gain stable suspension for a rotor, some degrees of freedom must be actively controlled. (Lantto, 1999) In mechanics, there are six degrees of freedom in total: elevating (y-axis), strafing (x-axis), walking (z-axis), yawing (rotation around x-axis), pitching (rotation around y-axis) and rolling (rotation around z-axis).

In active magnetic bearing supported high speed machines, the levitation of the rotor is typically achieved with three magnetic bearings: two radial bearings and one axial bearing. The radial bearings are placed on each end of the rotor; their function is to support the rotor in radial directions while reducing rotation around x- and y-axes. The magnetic pull generated by the radial bearings is perpendicular to the longitudinal axis of the rotor. The axial bearing prevent rotor from moving in the direction of the longitudinal z-axis. In such a system, five degrees of freedom are controlled (Gräsbeck, 2018). The function of a radial magnetic bearing can be integrated to the motor itself, so that it generates radial forces as well as rotational torque. A system like this is called bearingless or self-bearing machine. (Chiba, et al., 2005)

This bachelor's thesis focuses on the radial control of a bearingless machine with four degrees of freedom (4-DOF) i.e., movement in the directions of x- and y-axes and the rotation around x- and y-axes. The goal is to design a PID-based control system that is capable of stabilizing the rotor in perpendicular directions while removing rotation around x- and y-axes. The mathematical model of the system is brought together so that position stiffness and current stiffness of the system are linearized to allow linear examination. Thus, the linear model is used for the control design.

MATLAB® is used to tune the controllers. The modeling of the system is carried out in Simulink® environment. After tuning, modeling and simulating the system, the control model is tested in practice with a 10 kW 5-DOF bearingless machine.

2 MAGNETIC LEVITATION

In this section, a short review of magnetic levitation and its development is given. In addition, an introduction to bearingless machines is given.

2.1 A SHORT HISTORY OF MAGNETIC LEVITATION

The magnetic levitation is based on the attraction between ferromagnetic bodies, where the object is suspended with only the use of magnetic fields. (Han & Kim, 2016) The authors would like to state that there has been a long history of research in this field, and for that reason, only a short overview is given.

Earnshaw published his theorem in 1842 wherein he proved that any open looped magnetic levitation system could not gain stable suspension (Earnshaw, 1842). Since its publishing, it took almost a century for technology to advance, which eventually led to such inventions as "*monorail vehicle with no wheels attached*" (Kemper, 1934) and the advancements around centrifuges (Holmes & Beams, 1937). One should also note Beams advances in magnetic bearings with patents such as "*suspension of rotatable bodies*" (Beams, 1938). These innovations led to the discoveries such as magnetic levitation train technology (Fig. 2.1) and active magnetic bearings. (Han & Kim, 2016; Polajžer, 2010)

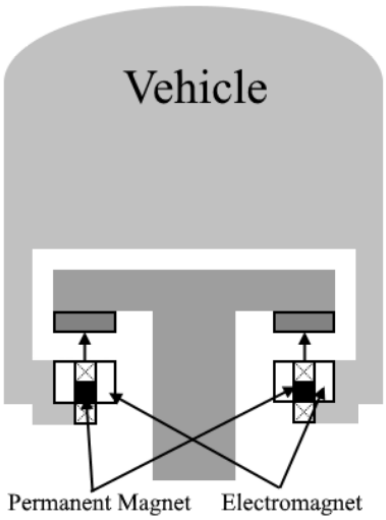

Figure 2.1. Hybrid magnetic suspension i.e., the use of both passive and active magnets. In general, vehicles using magnetic levitation technology may have hybrid magnetic suspension similar to the idea presented here.

The modern magnetic bearings with digital control were made possible with the development of solid-state electronics and modern computer-based control technology by Habermann (Habermann & Liard, 1979) and Schweitzer (Schweitzer & Lange, 1976). Magnetic bearings are used to support all kinds of ferromagnetic objects e.g., rotors. Magnetic bearings are often divided into three categories: passive magnetic bearings (PMBs), active magnetic bearings (AMBs) and hybrid magnetic bearings (HMBs). (Schweitzer, et al., 2009)

The PMBs are based on permanent magnets. Thus, they cannot be actively controlled so their applications are scarcer than AMBs. The PMBs can be utilized within the limits introduced in Earnshaw's theorem e.g., flywheels and bearingless machines (Bleuler, et al., 2005). The AMBs are based on electromagnets. Their active control is used in processes and applications where it is advantageous e.g., high speed machines, magnetic levitating vehicles and uranium enrichment. (Chiba, et al., 2005) On the contrary, the HMBs are a mixture of permanent magnets and electromagnets e.g., permanent magnet biased magnetic bearings (Fig. 2.2). The PMBs present no power loss due to the absence of current, but then again AMBs can be controlled and they possess higher stiffness. The HMBs are designed to combine the merits of both PMBs and AMBs (Jiancheng, et al., 2009). (Rai, et al., 2016)

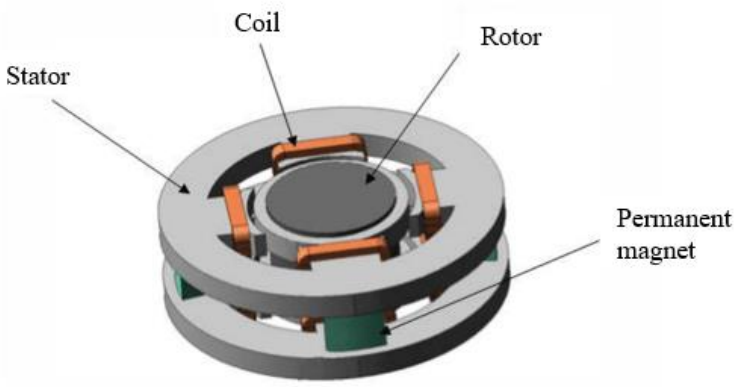

Figure 2.2. Radial permanent magnet biased AMBs. The use of permanent magnets lowers the startup power spike. (Kandil, et al., 2016)

It should be noted that the use of diamagnetic materials in magnetic bearings is possible, although this field remains relatively undeveloped, and therefore its uses are still very scarce. (Cansiz & Hull, 2004)

The levitation for bearingless machines is done with the use of integrated levitation coils and can have an external axial magnetic bearing. The bearingless machines are hybrids of magnetic bearings and electric motors (Oshima, et al., 1996). (Chiba, et al., 1994)

2.2 PROPERTIES OF MAGNETIC BEARINGS AND BEARINGLESS MACHINES

In this section, a review of the properties in magnetic bearings and bearingless machines is given. A common practice in magnetic levitation is to use magnetic bearings to generate magnetic suspension. The so-called conventional magnetic bearings have four static electromagnets placed around a rotating shaft; this enables radial control in the directions of x- and y-axes (Schweitzer, et al., 2009). Having no physical contact with the magnetic bearings makes the rotor have no wear, and therefore lubrication is not required. (Chiba, et al., 2005)

When separate radial bearings are placed at both ends of the rotor, the rotor needs to be longer than that in a bearingless machine, where integrated levitation coils are used. This can lead to problems such as high rotor elasticity. Even though the elasticity of a rotor can be reduced, the integrated levitation coils are often more preferred solution. (Majewski, et al., 2007; Chiba, et al., 2005)

In a rotor with rigid body, the distance between any two given points remain the same i.e., there is no bending regardless of any external forces exerted on it. (Chiba, et al., 2005; Oshima, et al., 1996) Fig. 2.3 represents a traditional AMB supported high speed motor.

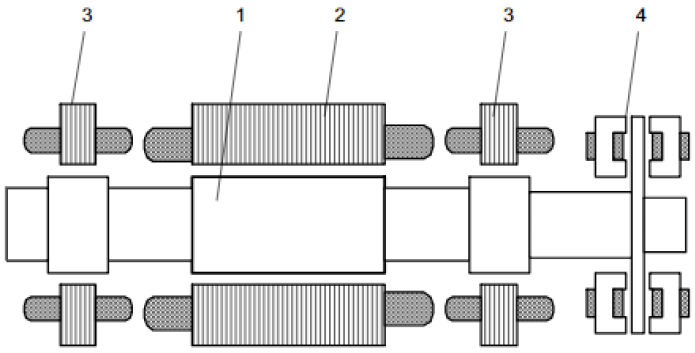

Figure 2.3. Rotor with high speed passive magnet brushless motor and magnetic bearings: 1. rotor, 2. stator, 3. radial AMBs, 4. axial AMB. Adapted from (Gieras, 2010).

In a bearingless drive, the function of a magnetic bearing is integrated into the motor itself to create a bearingless unit, which generates radial forces as well as rotational torque. This integration makes the system more compact and allows the use of a shorter rotor. Bearingless machines also require fewer inverters than systems with magnetic bearings. It should be noted that bearingless machines function well in vacuums and sterile environments because of their characteristics. In addition, being able to dampen down vibrations is often sought

after property in these high frequency systems and the ability is more noticeable in systems with active suspension. (Schweitzer, et al., 2009; Chiba, et al., 1994)

The complexity of bearingless machines offers a multitude of freedoms in constructive design. Different machine setups may have nearly the same dynamic behavior and may differ only slightly in their operation characteristics. The common bearingless machine consists of motors such as permanent magnet motor, switched reluctance motor, induction motor, salient-pole synchronous motor, or cylindrical rotor synchronous motor accompanied by integrated levitation coils or external magnetic bearings. (Chiba, et al., 1994; Silber, et al., 2005; Oshima, et al., 1996)

2.2.1 Permanent magnets

Permanent magnets offer strong attractive forces without the use of power. Permanent magnets can be utilized in variety of applications due to their compactness, reliability and very long lifetime. (Yonnet, 1978)

Fig. 2.4 represents radial passive magnetic bearing system, where a rotor is being attracted to both negative and positive directions of y-axis making it stable in perpendicular directions.

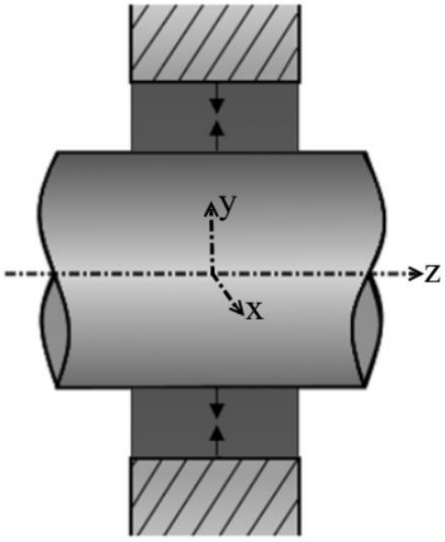

Figure 2.4. Radial permanent magnet bearing suspending a rotor with attractive forces.

The magnetic pull force of a single permanent magnet depends on their magnetic flux density *B* or their magnetizing field *H*, the cross-sectional area of the magnetic poles *A* and the permeability of vacuum μ_0

$$f_{\mathrm{m}} = \frac{B^2 A}{2\mu_0} = \frac{\mu_0 H^2 A}{2}. \quad (2.1)$$

The (2.1) works also with electromagnets. (University of Surrey, 2010)

2.2.2 Electromagnets

Fig. 2.5 represents a basic 1-DOF AMB control loop. The control loop consists: 1. rotor, 2. sensor, 3. controller, 4. power amplifier and 5. electromagnet.

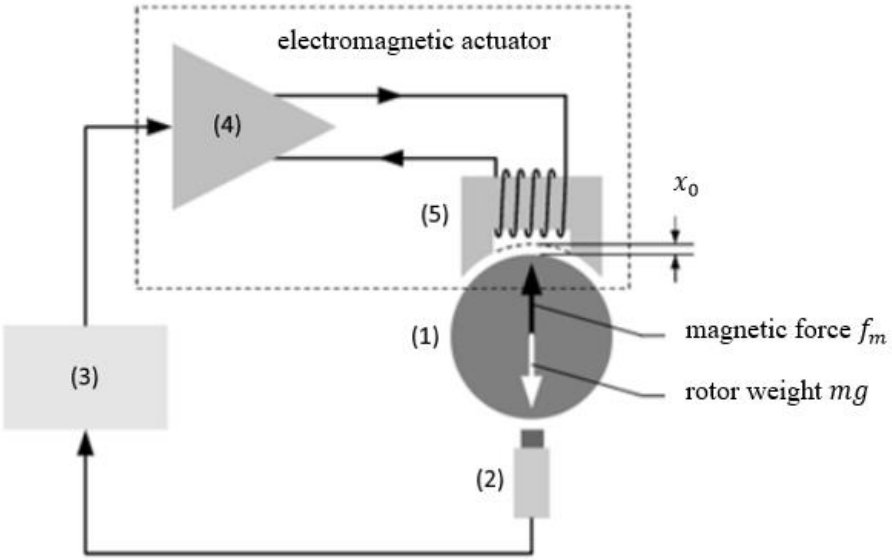

Figure 2.5. The basic AMB control loop and its elements. Adapted from (Schweitzer, et al., 2009).

The magnetic pull f_m generated by the electromagnet and earth's gravitational pull $f_g = mg$ are tried to be kept in balance. The sensor measures the displacement of the rotor from intended air gap x_0 and feeds the information to the controller. The controller's purpose is to maintain the rotor's place at its intended position. In addition to balancing the affecting forces, the controller must stabilize the system i.e., dampen fast movements of the rotor and reduce steady state error. Finally, the controller sends out a current command signal to the power amplifier, which transforms this signal into control current for the coil, thus generating desired magnetic force f_m. (Schweitzer, et al., 2009)

When modeling the system, several forces and laws of nature must be considered. To simplify the model of the system, neither dynamics of the sensor nor electronics of the power amplifier are to be taken into account. Although, these must be taken account in the final simulation model.

Despite the strong nonlinearities, the AMB systems can be controlled with a linear control system. Thus, the position and the current stiffness of the magnetic pull f_m must be linearized at the operating point (x_0, i_0, mg) as displayed in Fig. 2.6. (Schweitzer, et al., 2009) Resulting linearized model only works in the close proximity of the operating point (Larjo, 2006).

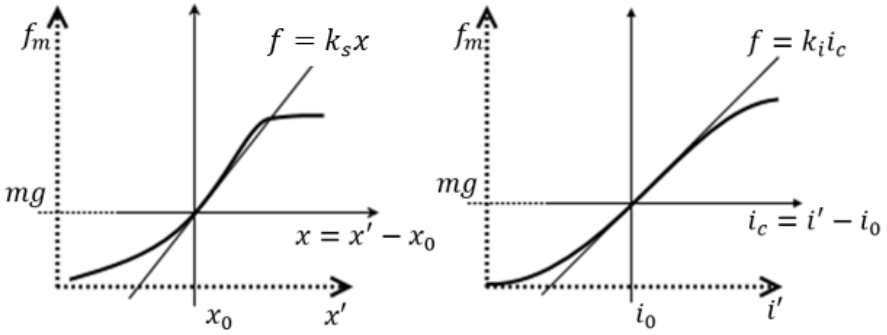

Figure 2.6. Linearization at the operating point: (left) relationship between force and displacement i.e., position stiffness; (right) relationship between force and current i.e., current stiffness.

To eliminate all operating point quantities from the resulting equations new variables are introduced for the force f, the control current i_c and the displacement x as follows

$$f = f_m - f_g, \tag{2.2}$$

$$i_c = i' - i_0, \tag{2.3}$$

$$x = x' - x_0, \tag{2.4}$$

where f_m is the magnetic pull of the electromagnet, f_g is the earth's gravitational pull, i' is the current in the coil, i_0 is the constant bias current, x_0 is the intended length of the air gap between the electromagnet and the rotor and x' is the displacement from said x_0. The value of x' is limited to the length of the air gap at given time. (Schweitzer, et al., 2009)

Linearizing the system yields the following equation for produced force at the operating point

$$m\ddot{x} = k_s x + k_i i_c, \tag{2.5}$$

where m is the mass affecting the bearing, $\ddot{x}$ is the acceleration of gravity, k_s is the position stiffness and k_i is the current stiffness. How the forces actually affect the rotor can be found in Fig. 2.7. (Schweitzer, et al., 2009)

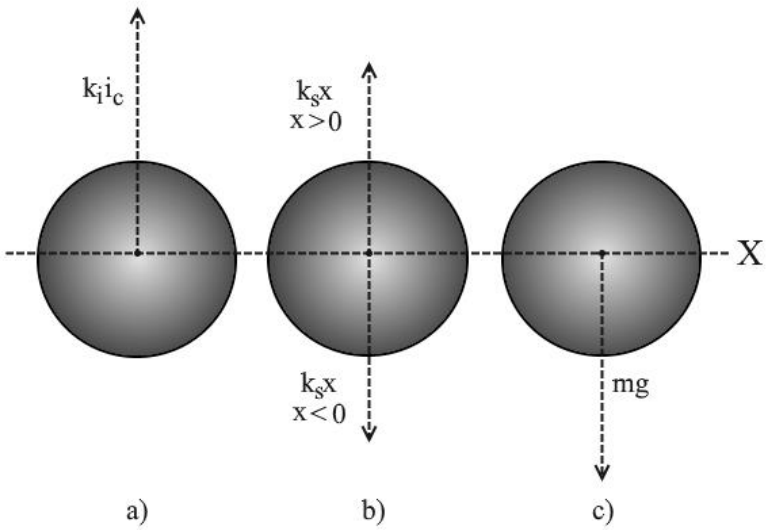

Figure 2.7. Forces affecting a rotor: a) Magnetic pull produced in the electromagnet, b) Force aiding or resisting the magnetic pull depending on the displacement i.e. when $x < 0$ the force is resisting the pull and when $x > 0$ the force is aiding the magnetic pull, c) Constant force generated by the mass of the rotor and the acceleration of gravity.

To make an AMB system stable it needs to be actively controlled. To stabilize the system, a control law is needed, which purpose is to send out current command signals that result in force vectors f_{m} and f_{g} cancelling each other (Fig. 2.8).

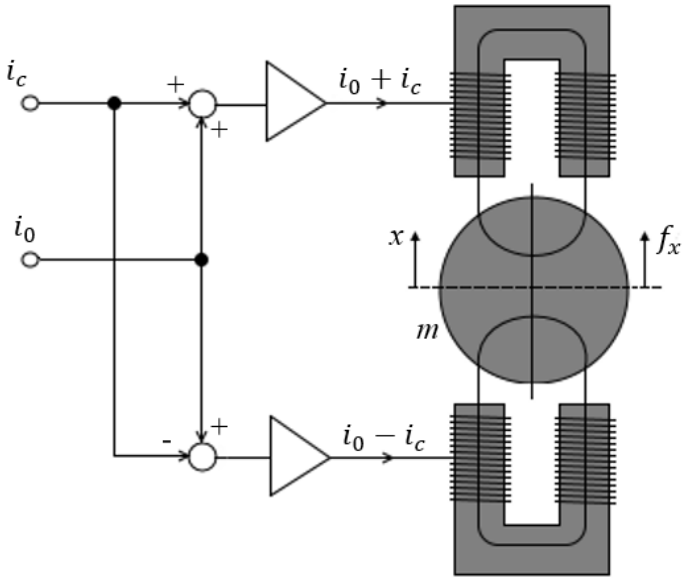

Figure 2.8. Active magnetic bearing system with one degree of freedom, where the forces are caused by the opposite electromagnets and gravitation. Control current i_{c} is the output of the control system; i_0 is the constant biasing current.

Usually, the rotor's radial axis is controlled with two electromagnets on opposite sides; this enables the production of both the positive and negative forces. The upper electromagnet is

controlled with the sum of constant bias current i_0 and control current i_c and the lower electromagnet with their subtraction. (Kurvinen, 2016)

The electromagnetic pull for U-shaped electromagnet is calculated by

$$f_m = \frac{1}{4}\mu_0 N^2 A \frac{i'^2}{x^2}, \tag{2.6}$$

where N is the number of loops in coil and A is the projected area by the electromagnet. (Kurvinen, 2016)

In practice, radial magnetic bearings have magnetic forces affecting the rotor in an angle of α. This is due to the deviation in the angle of the magnetic force in relation to the gravitational pull. Sometimes it is intentional to distribute the weight of the rotor. Thus, the magnetic force is

$$f_m = k\frac{i'^2}{x^2}\cos(\alpha), \tag{2.7}$$

with stiffness *k*

$$k = \frac{1}{4}\mu_0 N^2 A. \tag{2.8}$$

(Hynynen, 2011)

The force f_x is achieved in the direction of x-axis; it represents the difference between the forces pulling from opposite directions. Therefore, force f_x can be evaluated with

$$f_x = f_+ - f_- = k\left(\frac{(i_0+i_c)^2}{(x_0-x)^2} - \frac{(i_0-i_c)^2}{(x_0+x)^2}\right)\cos(\alpha), \tag{2.9}$$

Linearizing (2.9) with the presumption that $x \ll x_0$ yields

$$f_x = \frac{4ki_0}{x_0^2}\cos(\alpha)\, i_c + \frac{4ki_0^2}{x_0^3}\cos(\alpha)\, x = k_s x + k_i i_c. \tag{2.10}$$

When assumed that the cross-sectional areas of the magnet A_{fe} and the air gap A_a are equal, the position stiffness and the current stiffness can be defined with (2.11) and (2.12)

$$k_{\mathrm{i}} = \frac{4ki_0}{x_0^2}\cos(\alpha) = \frac{AN^2\mu_0 i_0}{x_0^2}\cos(\alpha), \tag{2.11}$$

$$k_{\mathrm{s}} = \frac{4ki_0^2}{x_0^3}\cos(\alpha) = \frac{AN^2\mu_0 i_0^2}{x_0^3}\cos(\alpha). \tag{2.12}$$

(Schweitzer, et al., 2009)

2.2.3 2-DOF system with radial active magnetic bearing

Fig. 2.9 represents a practical AMB control loop; it shares all the same elements as the system in Fig. 2.8, but with the addition of one axis and tilting of 45 degrees. The reasoning behind tilting the bearing is to distribute the weight of the rotor to both axes. When the bearing is tilted 45 degrees in respect to gravitational pull, it enables symmetrical control for both axes, with each axis supporting $1/\sqrt{2}$nd part of the rotors weight.

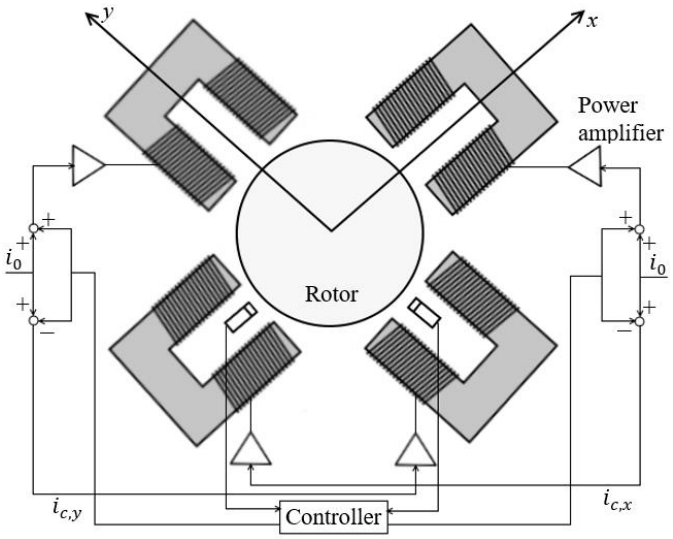

Figure 2.9. Radial active magnetic bearing system with two degrees of freedom tilted in 45 degrees.

Resulting forces for f_{x} and f_{y} become

$$f_{\mathrm{x}}(i_{\mathrm{c,x}}, x) = k\left(\frac{(i_0+i_{\mathrm{c,x}})^2}{(x_0-x)^2} - \frac{(i_0-i_{\mathrm{c,x}})^2}{(x_0+x)^2}\right)\cos(\alpha), \tag{2.13}$$

$$f_{\mathrm{y}}(i_{\mathrm{c,y}}, x) = k\left(\frac{(i_0+i_{\mathrm{c,y}})^2}{(x_0-x)^2} - \frac{(i_0-i_{\mathrm{c,y}})^2}{(x_0+x)^2}\right)\cos(\alpha). \tag{2.14}$$

(Gräsbeck, 2018)

3 BEARINGLESS MACHINES

In this section, a review of control design, modeling and cross-coupling in bearingless machines are given. In addition, the properties of the used test rig and the values used in simulations are presented. The examination focuses on 4-DOF magnetic levitation system with a rigid rotor. Even though the modelling of the system is examined as an AMB supported rotor and AMB terminology is used, the designed position controller can be used in the actual test rig, which uses bearingless motors instead of AMBs.

3.1 4-DOF SYSTEM WITH RADIAL ACTIVE MAGNETIC BEARINGS

Fig. 3.1 represents the principle behind the degrees of freedom that a system with two radial AMBs withholds when longitudinal movement is disregarded. The system acts like two separate 2-DOF systems when the cross-coupling is not considered i.e., both radial AMBs act as separate units.

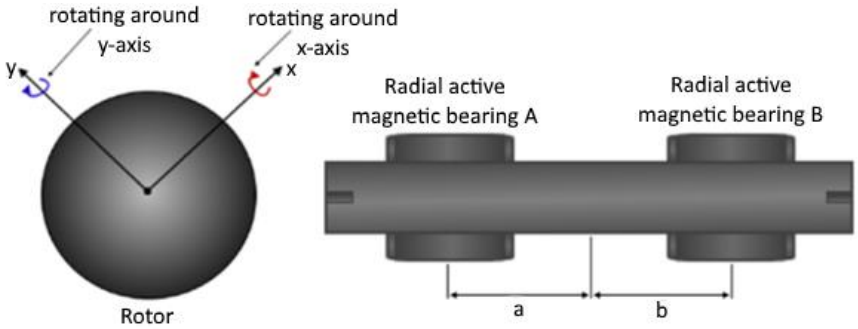

Figure 3.1. Radial active magnetic bearing system with four degrees of freedom and a rigid rotor.

In a typical symmetrical configuration, the rotor is supported with two radial magnetic bearings placed within the same distance of the rotor's center of mass. Although, there are cases where asymmetry is preferable i.e., systems where the rotor's center of mass is not in the middle. The electromagnets that generate forces in the direction of x-axis are controlled with currents $i_{\mathrm{c,xA}}$ and $i_{\mathrm{c,xB}}$. The forces parallel to y-axis are controlled with currents $i_{\mathrm{c,yA}}$ and $i_{\mathrm{c,yB}}$. (Schweitzer, et al., 2009)

The input for the model is bearing force

$$\boldsymbol{F}_{\mathrm{b}} = \left[f_{\mathrm{xA}}, f_{\mathrm{yA}}, f_{\mathrm{xB}}, f_{\mathrm{yB}}\right]^{T}, \tag{3.1}$$

and the output is the position vector

$$\boldsymbol{z}_{\mathrm{b}} = [x_{\mathrm{A}}, y_{\mathrm{A}}, x_{\mathrm{B}}, y_{\mathrm{B}}]^T. \tag{3.2}$$

The equation of motion for the rotor can be written

$$\mathbf{M}_{\mathrm{b}}\ddot{\boldsymbol{z}}_{\mathrm{b}} = \boldsymbol{F}_{\mathrm{b}} + \mathbf{F}_{\mathrm{g}}, \tag{3.3}$$

where $\mathbf{M}_{\mathrm{b}}$ is the mass matrix of the rotor, $\boldsymbol{F}_{\mathrm{b}}$ is the bearing force vector and $\mathbf{F}_{\mathrm{g}}$ is the force vector caused by the rotor's mass. It should be noted that the gyroscopic effect is considered insignificant, and therefore it is not taken into account. In the model, the x- and y-axes have been tilted 45 degrees in respect to gravitational pull, as seen in Fig. 3.1, which results in

$$\boldsymbol{F}_{\mathrm{g}} = -\frac{mg}{\sqrt{2}(a-b)}[-b \quad -b \quad a \quad a]^T, \tag{3.4}$$

where m is the rotor's mass, g is the acceleration of gravity, a is the distance from bearing A to the rotor's center of the mass and b is the distance from bearing B to the center of the mass (Fig. 3.1).

For state model presentation, a linearized vector $\boldsymbol{F}_b$ can be used

$$\boldsymbol{F}_{\mathrm{b}} = \mathbf{K}_{\mathrm{s}}\boldsymbol{z}_{\mathrm{b}} + \mathbf{K}_{\mathrm{i}}\boldsymbol{i}_{\mathrm{c}}, \tag{3.5}$$

where $\mathbf{K}_{\mathrm{s}}$ is the position stiffness matrix, $\mathbf{K}_{\mathrm{i}}$ is the current stiffness matrix and $\boldsymbol{i}_{\mathrm{c}}$ is the control current vector. The force caused by the rotor's mass is invariable, so it can be compensated with constant current $\boldsymbol{i}_{\mathrm{cg}}$

$$\boldsymbol{i}_{cg} = -\mathbf{K}_{\mathrm{i}}^{-1}\mathbf{F}_{\mathrm{g}}. \tag{3.6}$$

By stating that $\boldsymbol{i}_{\mathrm{c}} = \boldsymbol{i}_{\mathrm{c}} + \boldsymbol{i}_{\mathrm{cg}}$ the equation of motion (3.3) can be expressed as

$$\mathbf{M}_{\mathrm{b}}\ddot{\boldsymbol{z}}_{\mathrm{b}} = \mathbf{K}_{\mathrm{s}}\boldsymbol{z}_{\mathrm{b}} + \mathbf{K}_{\mathrm{i}}\boldsymbol{i}_{\mathrm{c}}, \tag{3.7}$$

where $\mathbf{M}_{\mathrm{b}}$ is the mass matrix with respect to bearings' frame of reference. The $\mathbf{M}_{\mathrm{b}}$ can be found with the following

$$\mathbf{M}_{\mathrm{b}} = \mathbf{T}^{-\mathrm{T}}\mathbf{M}_{\mathrm{c}}\mathbf{T}^{-1}, \tag{3.8}$$

where $\mathbf{M}_\mathrm{c}$ is the mass matrix with respect to the rotor's center of mass

$$\mathbf{M}_\mathrm{c} = \begin{bmatrix} J & 0 & 0 & 0 \\ 0 & m & 0 & 0 \\ 0 & 0 & J & 0 \\ 0 & 0 & 0 & m \end{bmatrix}, \tag{3.9}$$

and $\mathbf{T}$ is the transformation matrix

$$\mathbf{T} = \begin{bmatrix} -a & 1 & 0 & 0 \\ 0 & 0 & a & 1 \\ -b & 1 & 0 & 0 \\ 0 & 0 & b & 1 \end{bmatrix}. \tag{3.10}$$

The constant J found in (3.9) is the rotor's inertia. (Larjo, 2006; Schweitzer, et al., 2009)

3.1.1 State-space representation

In this section, a state-space representation of the system is given for the control design and the simulation implementation. The general equations for a continuous time-invariant state-space model are

$$\dot{\boldsymbol{x}}(t) = \mathbf{A}\boldsymbol{x}(t) + \mathbf{B}\boldsymbol{u}(t), \tag{3.11}$$

$$\boldsymbol{y}(t) = \mathbf{C}\boldsymbol{x}(t) + \mathbf{D}\boldsymbol{u}(t), \tag{3.12}$$

where $\boldsymbol{x}$ is the state vector, $\boldsymbol{u}$ the input vector and $\boldsymbol{y}$ the output vector of the system. $\mathbf{A}$ is the system matrix, $\mathbf{B}$ is the input matrix, $\mathbf{C}$ is the output matrix and $\mathbf{D}$ is the feedforward matrix. (Larjo, 2006)

To make a state-space model, the differential (3.7) can be expressed as

$$\boldsymbol{x} = \begin{bmatrix} \boldsymbol{z}_\mathrm{b} \\ \dot{\boldsymbol{z}}_\mathrm{b} \end{bmatrix}. \tag{3.13}$$

In addition, the second derivative $\ddot{\boldsymbol{z}}_\mathrm{b}$ needs to be solved from the (3.7) by multiplying it with $\mathbf{M}_\mathrm{b}^{-1}$ which gives

$$\ddot{\boldsymbol{z}}_\mathrm{b} = \mathbf{M}_\mathrm{b}^{-1}\mathbf{K}_\mathrm{s}\boldsymbol{z}_\mathrm{b} + \mathbf{M}_\mathrm{b}^{-1}\mathbf{K}_\mathrm{i}\boldsymbol{i}_\mathrm{c}. \tag{3.14}$$

The state equations become

$$\dot{\boldsymbol{x}} = \begin{bmatrix} 0 & \mathbf{I} \\ \mathbf{M}_\mathrm{b}^{-1}\mathbf{K}_\mathrm{s} & 0 \end{bmatrix} \boldsymbol{x} + \begin{bmatrix} 0 \\ \mathbf{M}_\mathrm{b}^{-1}\mathbf{K}_\mathrm{i} \end{bmatrix} \boldsymbol{i}_\mathrm{c}, \tag{3.15}$$

$$\boldsymbol{y} = [\mathbf{I} \quad 0]\boldsymbol{x}. \tag{3.16}$$

(Larjo, 2006; Schweitzer, et al., 2009)

3.2 CROSS-COUPLING

In this section, a review of cross-coupling in 2-axis AMB systems is given. Cross-coupling is a phenomenon within the system that is caused by multiple inputs affecting one another's output. This phenomenon can be caused by gyroscopic effects or magnetic effects between the axes. In control systems, cross-coupling can be dealt with by adding a compensation structure to the control design to suppress or even remove its effects.

Fig. 3.2 represents a rotor that has a stationary coordinate reference frame (x-, y- and z-axes) and rotational coordinate references (i-, j- and k-axes) for the movement of the rotor. Alignment of k- and z-axes is the ideal situation, however, in reality there is always a slight difference: the angular position θ_y. Differences between the directions of the axes create moment N_y around y-axis. This also applies to x-axis with respect to θ_x and N_x. (Chiba, et al., 2005)

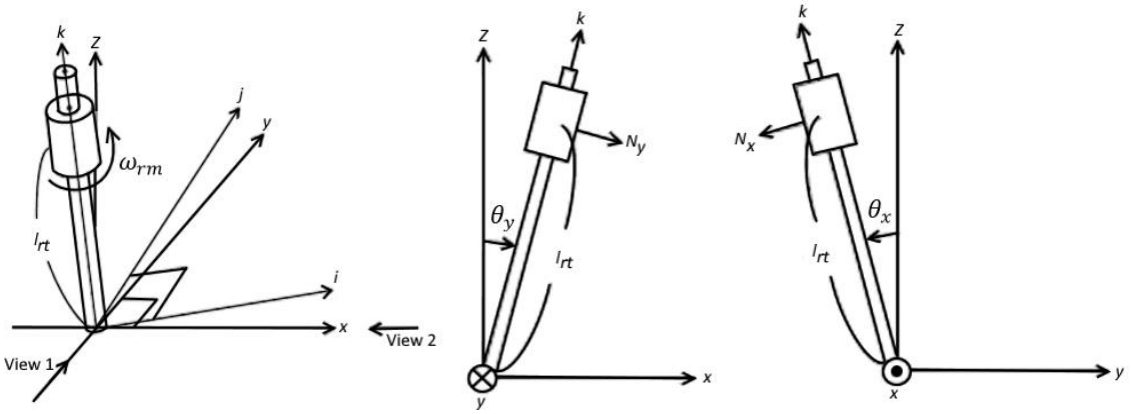

Figure 3.2. A view of the coordinate system, where the rotor is rotating around both x- and y-axis (left). Side views of the system are represented for y-axis (center) and x-axis (right). Adapted from (Chiba, et al., 2005).

3.3 BEARINGLESS PROTOTYPE MACHINE

Figs. 3.3, 3.4 and 3.5 represents the bearingless machine under study with integrated levitation coils. System dynamics of the prototype and the magnetic levitation created by bearingless motors can be presented with the theory found in Section 3.1. The bearingless prototype machine has the output of 10 kW. The tests are done with 5-DOF, where the rotation around z-axis is not being constrained.

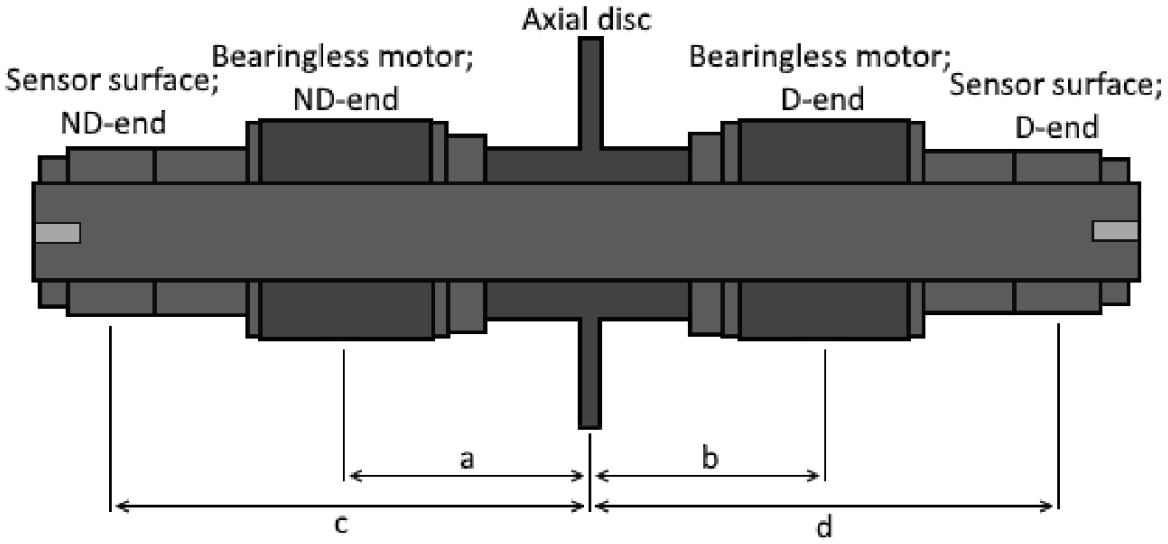

Figure 3.3. Cross-sectional view of the bearingless machine under study. ND-end stands for the non-driven end; D-end stands for the driven end.

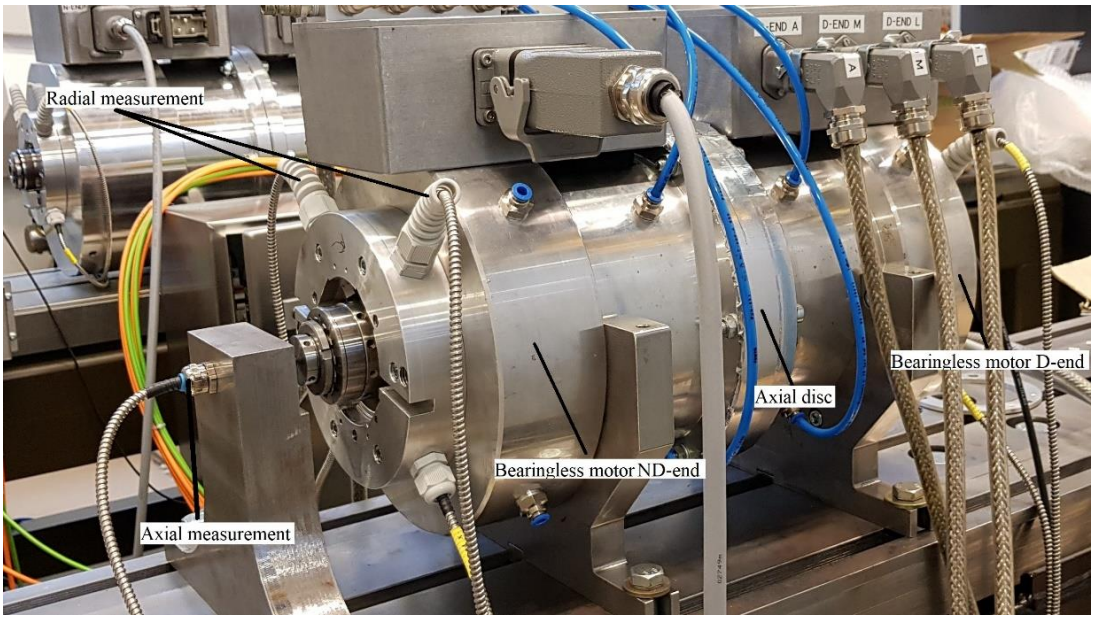

Figure 3.4. The bearingless machine under study.

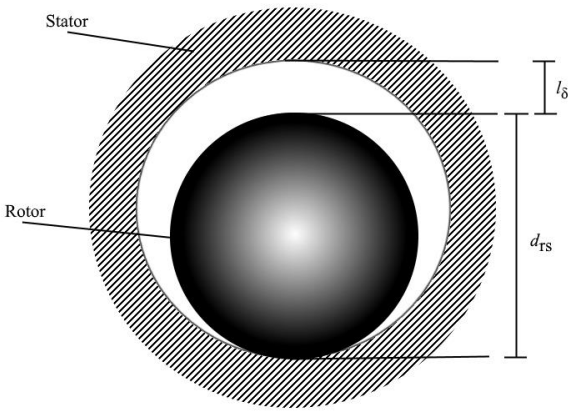

Figure 3.5. Cross-section of the bearingless motors with exaggerated dimensions.

The parameters for the prototype machine that are used in the control design and modeling of the system can be found in Table 1. Additional parameters can be found in Appendix 1.

Table 1. Parameters needed to model the system and design the controllers.

Parameter	Symbol	Value	Unit
Rotor mass	m	11.65	kg
Current stiffness, measured	k_{i}	29	N/A
Position stiffness, measured	k_{s}	672	N/mm
Bearingless motor location	a, b	107.5	mm
Rotor shaft diameter	d_{rs}	33	mm
Air gap length	l_δ	0.6	mm
Rotor inertia	J	0.232	kgm^2

3.4 CONTROL DESIGN

In this section, a review of single-input single-output (SISO) controllers in AMB systems is given. Additionally, the control design process will be presented along with proposed controller.

3.4.1 Control theory

Controllers get their input from the subtraction of position reference x_{ref} and measured displacement of the rotor *r*, which results in error signal *e*. The controller sends out a current command signal to the power amplifier, which changes the control current i_{c} accordingly. (Schweitzer, et al., 2009)

For any AMB system to be stable, it needs to be actively controlled using a feedback loop. A simple controller for a magnetic bearing is a PD controller (proportional-derivate)

$$C(s) = K_{\mathrm{p}} + K_{\mathrm{d}}s, \tag{3.17}$$

where *C*(s) is the transfer function, *s* is the Laplace variable, K_{p} is the proportional gain and K_{d} is the derivative gain. It has to be noted that the gains of P- and D-components affect the systems natural frequency ω_{n} and damping coefficient ξ. The connection between these quantities can be found

$$K_{\mathrm{p}} = \frac{m\omega_{\mathrm{n}}^2 + k_{\mathrm{s}}}{k_{\mathrm{i}}}, \tag{3.18}$$

$$K_{\mathrm{d}} = \frac{2m\omega_{\mathrm{n}}\xi}{k_{\mathrm{i}}}. \tag{3.19}$$

However, in practice a system that is controlled by a PD controller will have a noticeable steady state error e_{ss}, which results in inaccurate positioning of the rotor. In addition, the PD controller lacks the ability to correct position errors created by external forces. For these reasons, a PID controller (proportional-integral-derivate) is usually used in situations where the rotor is rigid. (Gräsbeck, 2018) In situations where the rotor is elastic, more advanced controller structure is more suitable. This is due to the flexible modes of the rotor.

The PID controller consists three parameters: P-, I- and D-components with their respected gains K_{p}, K_{i} and K_{d}. The P-component enables the current changes in the electromagnet's

coil, thus correcting the position of the rotor. The D-component reacts to fast changes i.e., it dampens them. The I-component is used to decrease static position error and through that reduces steady state error. The ideal transfer function of a parallel PID controller is

$$C(s) = K_\mathrm{p} + \frac{K_\mathrm{i}}{s} + K_\mathrm{d}s, \tag{3.20}$$

where K_i is the integral gain.

It is worth remarking that, the PID controller has a weakness: its ideal D-component amplifies high frequency noise. The high frequency noise from input affects output remarkably, so the use of ideal derivate is to be avoided in practice. Instead of using only ideal derivate, one should add a filter to sort out the high frequency noise

$$C_D(s) = \frac{K_\mathrm{d}s}{T_\mathrm{f}s+1}, \tag{3.21}$$

where T_f is the filter parameter. Now the high frequency amplification is limited to the value of $K_\mathrm{d}/T_\mathrm{f}$ and the aforesaid transfer function works as the derivate function in frequency zone of $1/K_\mathrm{d} \ll \omega \ll 1/T_\mathrm{f}$. (Chiba, et al., 2005; Wei & Söffker, 2016)

The new transfer function for the PIDf (proportional-integral-derivative-filter) controller comes out as

$$C(s) = K_\mathrm{p} + \frac{K_\mathrm{i}}{s} + \frac{K_\mathrm{d}s}{T_\mathrm{f}s+1}. \tag{3.22}$$

3.4.2 Design of the controllers

In this section, the design of the controllers and their relevant plots are given. This review will initially be conducted on a one axis system since it is more practical to view just one SISO system when all the axes are identical regarding their properties. In the final 4-DOF MIMO system, a decentralized PID-control is implemented so that there is one SISO controller for each degree of freedom. Although it should be noted that when applying the SISO controller to the multiple-input multiple-output (MIMO) system some further modifications are often needed for the best possible performance. (Åström & Hägglund, 1995)

Unlike the PD-controller, there are no analytical equations to determine fitting values for the PID-controlled system under study. The approach for the controller tuning is to use MATLAB® application "*PID Tuner*", which gives us approximate values to start with and offers more visual representation of the controller's components. However, one major problem with the values given by the *PID Tuner* is that the derivative gain tends to be too high for the system, so it would amplify high frequency noise too much.

Finalizing of the tuning is made by trial and error method whilst utilizing available control theory literature (Åström & Hägglund, 1995; Åström & Murray, 2008). After the tuning process yields results that are satisfactory, the controller will be simulated and its effects on the system are weighted. Position bandwidth will be interpreted from the gain crossover frequency (Hynynen, 2011). The design process will follow suit of Fig. 3.5.

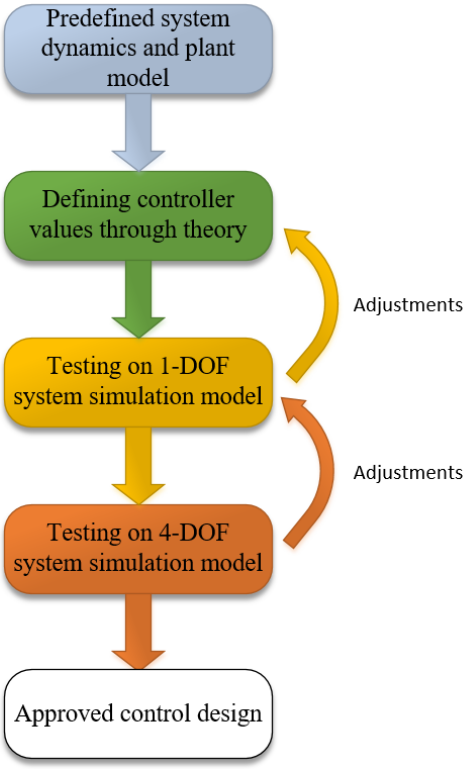

Figure 3.6. Flowchart of control design before test runs on the bearingless prototype machine.

A potential control design was found for the PIDf controller, values for it can be seen on Table 2.

Table 2. Proposed PIDf controller.

Variable	Value
K_{p}	42000
K_{i}	$8.2 \cdot 10^{5}$
K_{d}	103
T_{f}	$1 \cdot 10^{-3}$

Fig. 3.7 represents a Bode diagram for the 1-DOF mathematical model of the system with the proposed PIDf controller.

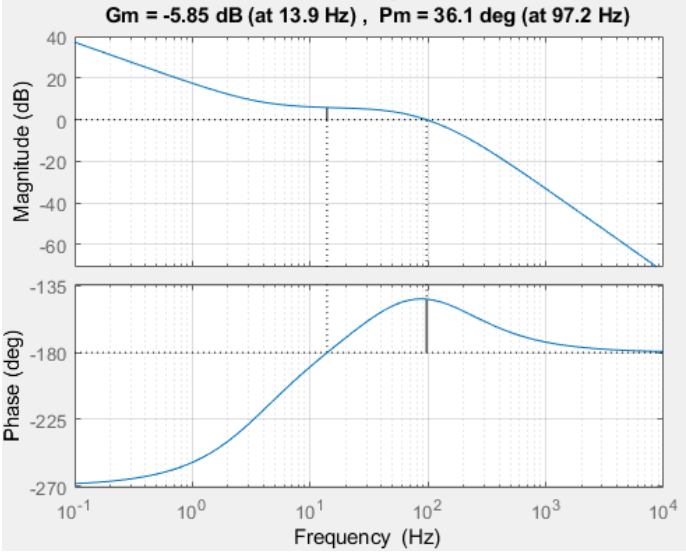

Figure 3.7. Bode diagram for the 1-DOF model.

The proposed controlled has position bandwidth of 134 Hz, phase margin of 36.1 degrees and gain margin of -5.85 dB. Although, the bandwidth is a fairly high, based on the simulations this controller has been selected as the initial controller to be ran on the system.

3.5 SIMULATION MODELS

In this section, the simulation models of AMB system with PID controllers are shown. It is remarked that the bearingless motor can be modeled using the same equations discussed above, and thus the simulation models are as in the case of AMB systems. This section will start with the simple 1-DOF system models and then it moves onto the 4-DOF model. It should be noted that when the electronics of the electromagnet and the current controller are not taken in to account, the control current is the output of the position controller.

3.5.1 1-DOF system model

Rotor's 1-DOF model, a single-point-mass model, without interference is presented in Fig. 3.8. The model can be derived based on the (2.5).

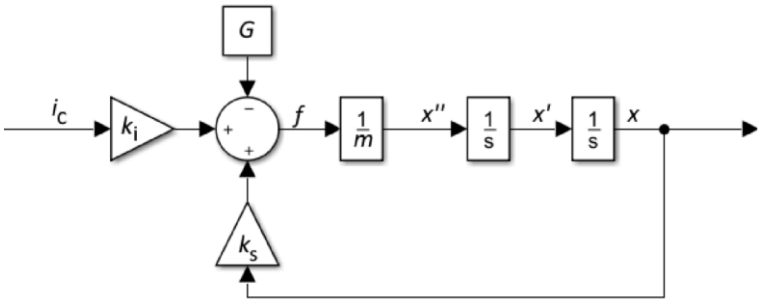

Figure 3.8. 1-DOF Rotor model.

Fig. 3.9 represents the model for 1-DOF PIDf controller that controls only one axis.

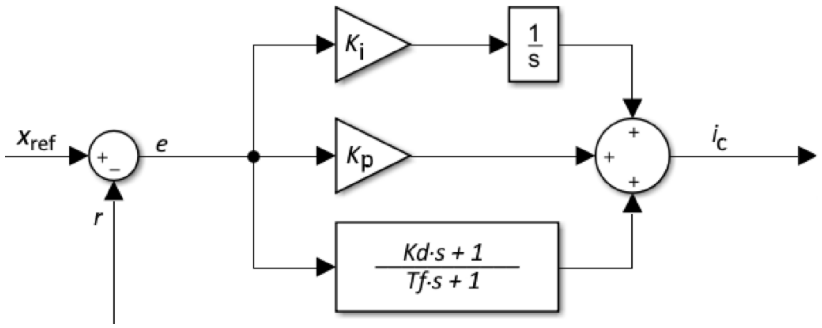

Figure 3.9. Model for SISO PIDf controller.

Fig. 3.10 represents the model of one axis system where both the rotor and the controller are incorporated. In addition, the effects of gravitation are modelled by constant force *G* that has opposite sign than magnetic pull f_m. The real system has a maximum current output, so the saturation block is used to limit the current in the Simulink® model. A current limit of 12 A has been selected in the simulations.

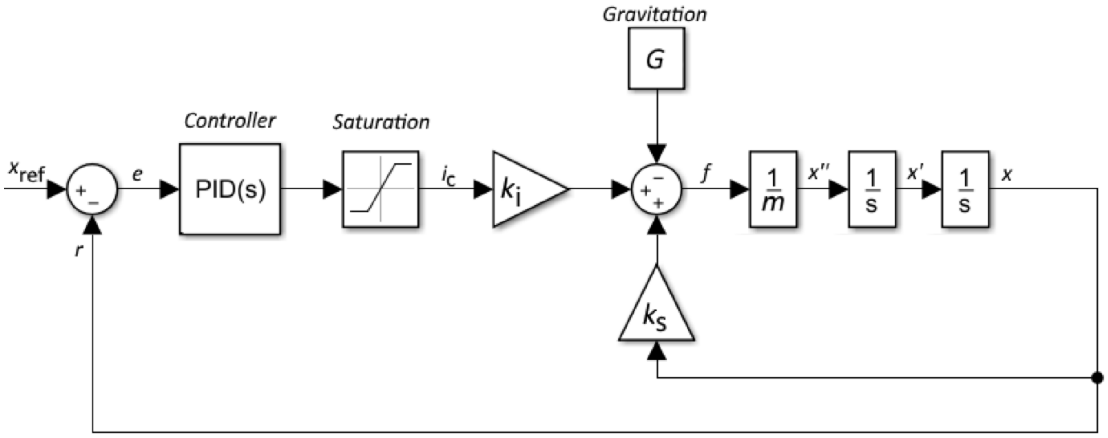

Figure 3.10. Control system for position control without noise or interference.

3.5.2 4-DOF system model

Fig 3.11 represents a 4-DOF position control system where the control is implemented with four separate, yet identical PIDf controllers with each of them controlling one DOF. The rotor's model is presented as a state space model (3.15) and (3.16) using Simulink® state-space block. Note that, there is no cross-coupling applied to the system. White noise is added to the simulation to represent the measurement noise in the system.

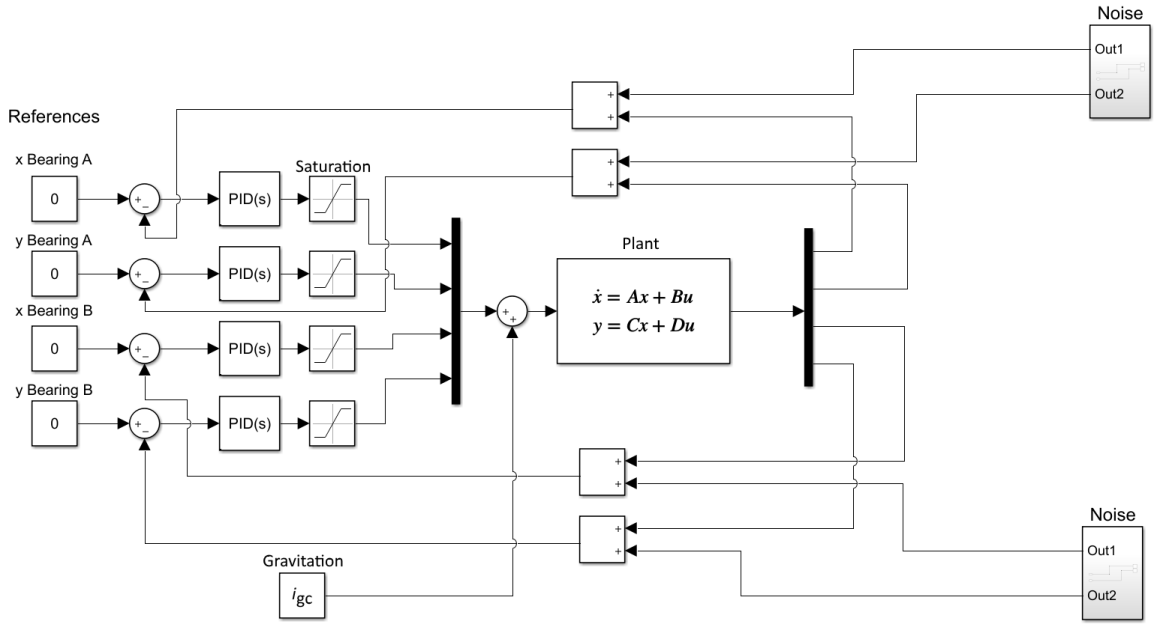

Figure 3.11. 4-DOF position control system. The initial position of the rotor is x_init = [0.0000942 -0.000428 0.000225 0.000366] m.

In the appendix 1, the prototype machine parameters can be found that are used to built the simulation model.

4 RESULTS

In this section, simulations and measurements on the bearingless prototype machine are performed using the proposed controller. Since the model is not completely accurate and it is missing some elements the real system has, there is no guarantee that the simulation behaves the same way as the actual system, thus the simulation results will be compared to the actual behavior of the system.

Bearingless motor A (D-end) acts as a modifiable end where force or displacement can be applied. Bearingless motor B (ND-end) remains unmodified throughout this review. The sensors are angled 45 degrees in respect to gravitation, so the measurements vary slightly when the measurement point is not perpendicular to the diameter of the rotor. The abbreviation BM stands for bearingless motor.

4.1 SIMULATED 4-DOF SYSTEM

The proposed PIDf controller will be tested on the 4-DOF system model. Fig. 4.1 represents the lift-up from the bearingless motor's point of view.

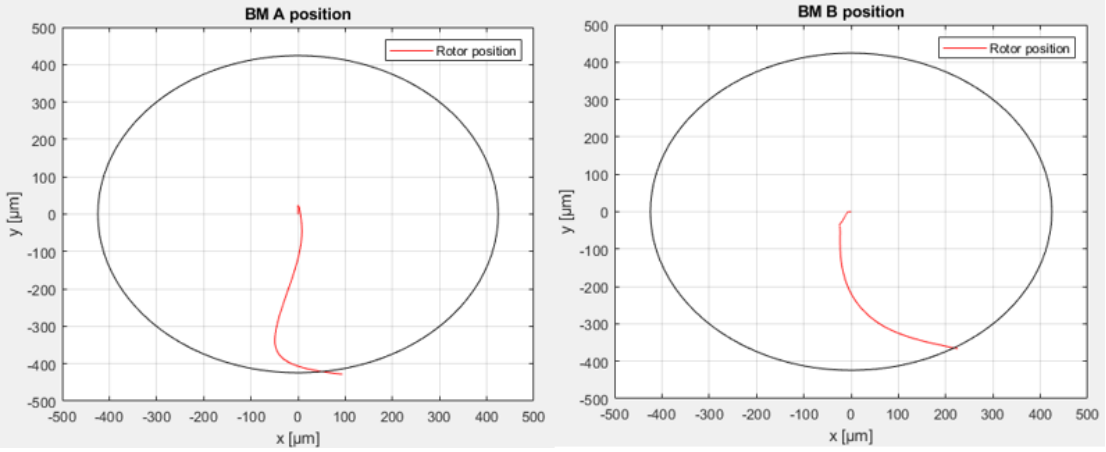

Figure 4.1. Simulated lift-up, initial positions are the same as in the test run done with the actual rig to have the most truthful situation. Radius of the circle is the air gap at center divided by cosine of 45 degrees.

From Fig 4.1 it can be noticed that, the lift-up was successful with small amount of overshoot; these results indicate that the overall gain of the controller could possibly be smaller to avoid any overshoot. Although in the actual system the current and the position stiffness are nonlinear, and for this reason, the overall gain cannot be too small.

4.2 COMPARISON BETWEEN MEASURED AND SIMULATED VALUES

The proposed controller is implemented to the control system of the bearingless prototype machine and the results are compared to those of the simulated 4-DOF system. Fig. 4.2 represents a comparison between the currents of the simulated system and the measured system during the lift-up.

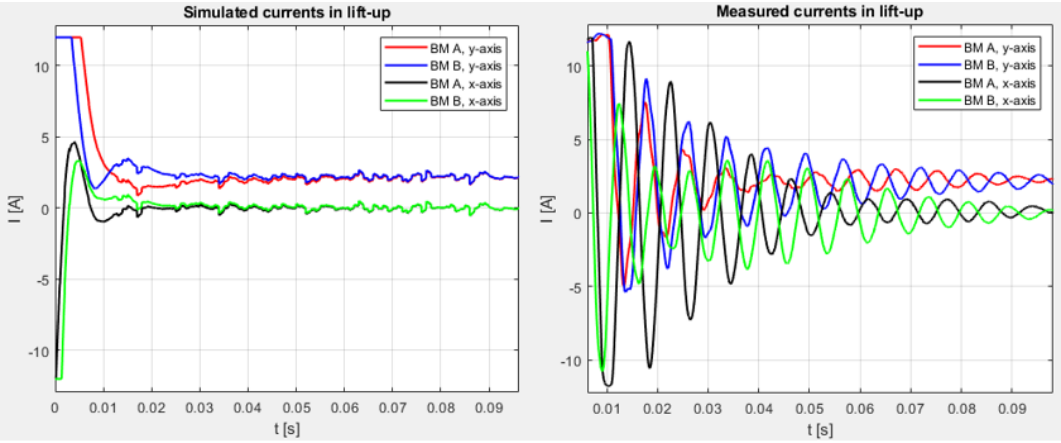

Figure 4.2. Comparison between the simulated currents and the measured currents during the lift-up.

It can be observed that, the general trend for the graphs tends to be similar, but the results show that the steady state will be achieved slower in the plots with the test run data. The measured results also show unwanted transient behavior with the frequency of 125 Hz. The current spikes seen in the simulation currents at its steady state are caused by the noise block added to the Simulink® model. The transient behavior found could be the result of several reasons such as high overall gain, derivate gain, too wide position bandwidth that picks up noise from the system or it could be caused by the cross-coupling. It can be assumed that, the vibration is most likely caused by the controller design that requires more experimental tuning.

Fig. 4.3 represents a position comparison between the positions of the simulated system and the measured system.

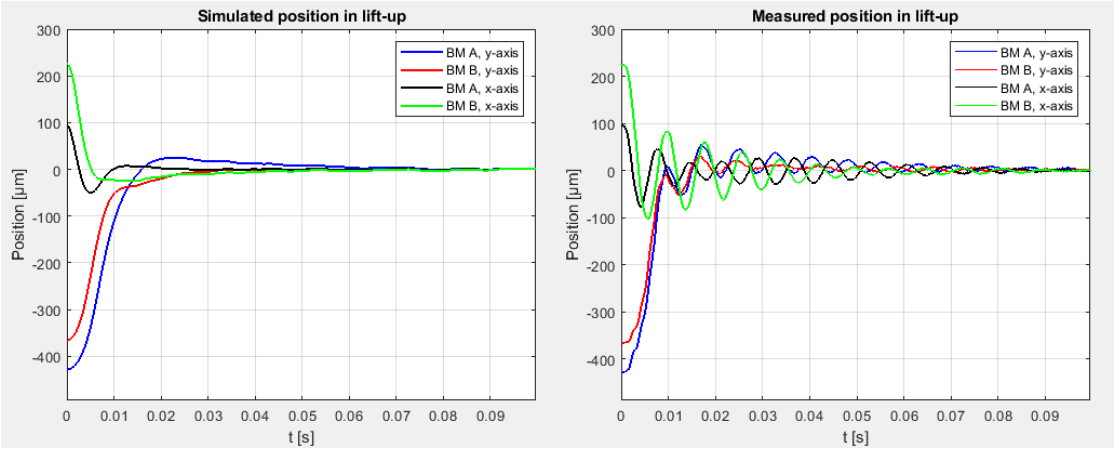

Figure 4.3. Comparison between simulated positions and measured positions during the lift-up.

There is also transient behavior in the rotor's position, which most likely is the result of its current. Obviously, the rotor oscillates with the same 125 Hz frequency as the current. When the system is set to have 1% error margin the measured system has a settling time of 95ms. The simulation has a settling time of 73ms. The steady state error is calculated from the largest possible air gap between the sensor and the rotor when they align perpendicularly, which is air gap divided by cos(45).

Fig. 4.4 represents a comparison of the simulated and the measured lift-ups.

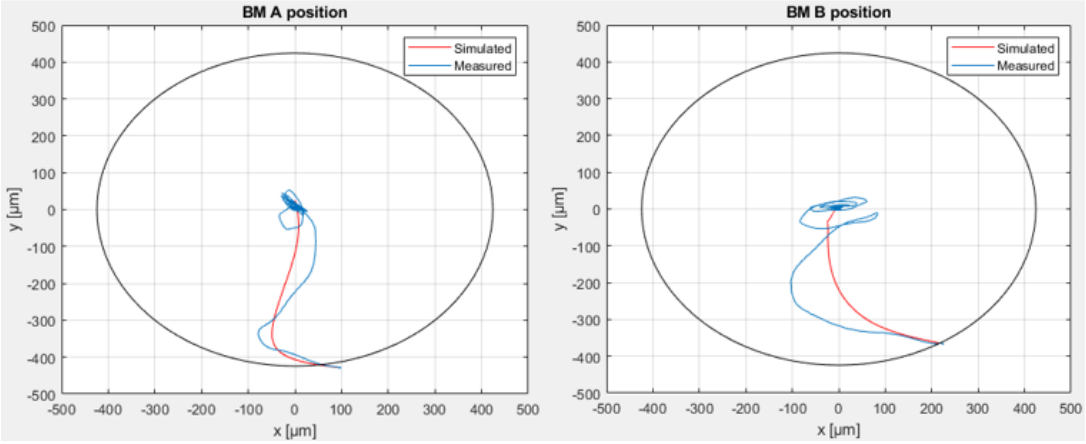

Figure 4.4. Measured lift-up with proposed controller. On the left are the lift-ups in bearingless motor A and on the right the lift-ups in bearingless motor B.

By comparing the results, it can be noticed that the experimental results also provide successful lift-up with a small overshoot. After the rotor reaches the center of the stator the system acts closest to the linearized model.

Fig. 4.5 represents the rotor position when a displacement of 50 µm is applied to the positive direction of y-axis only for the bearingless motor A.

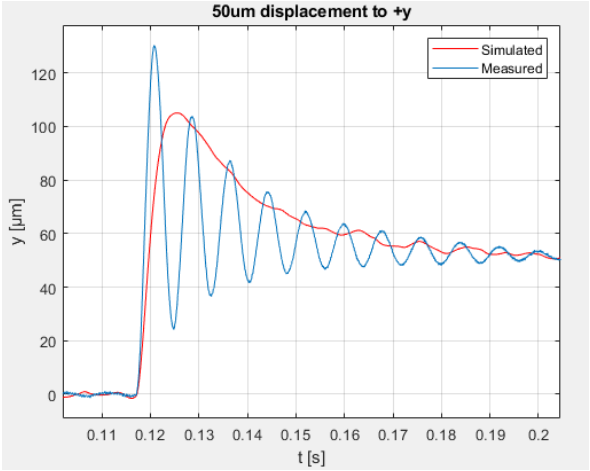

Figure 4.5. Comparison between simulated and measured values when 50 µm displacement is applied to the positive y-axis.

The measured results in Fig 4.5 show similar transient behavior seen in previous figures, but it can be interpreted that the simulated model and the prototype machine behave similarly validating the used simulation model and the used controller. To be more specific, the trend of the simulated and measured step response is similar. The simulation has an overshoot of 110% while the measured results show an overshoot of 160%.

Fig. 4.6 represents the exact situation but shows the positions of both measurement points.

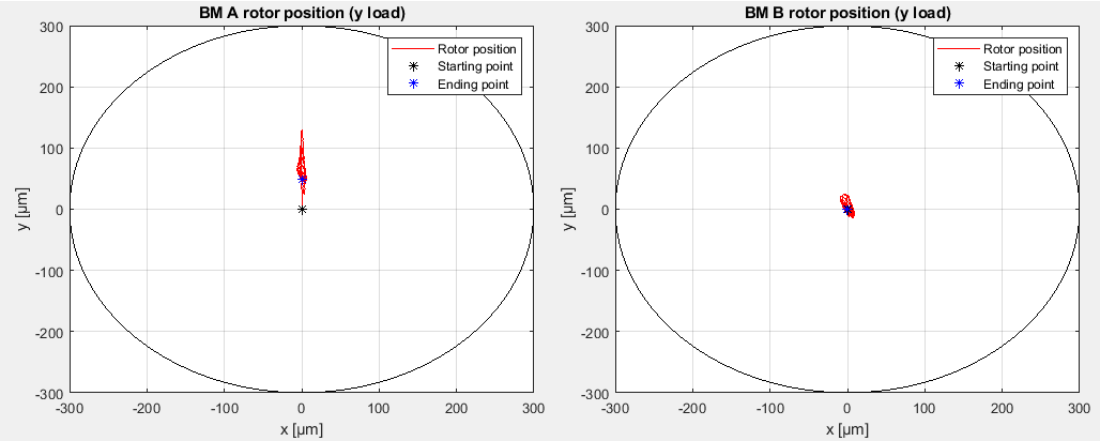

Figure 4.6. Rotor positions when a 50 µm displacement is applied to y-axis of the bearingless motor A.

Fig. 4.7 represents a situation where a displacement of 50 µm is applied to the positive direction of x-axis for bearingless motor A.

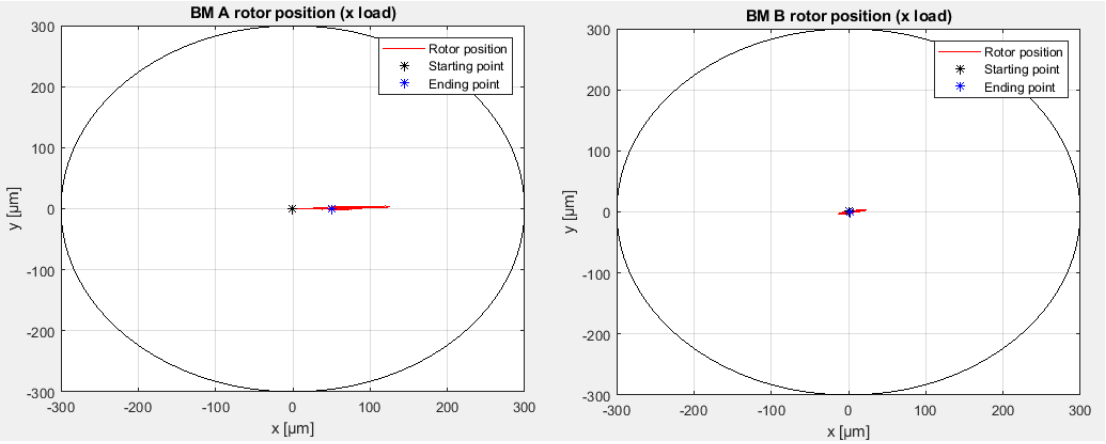

Figure 4.7. Rotor positions when a 50 µm displacement is applied to x-axis of bearingless motor A.

Both displacements result in similar trajectories, thus concluding that there are no strong nonlinearities overcoming one another. Even though the displacement was given only to the bearingless motor A, the rotor shows movement on the side of the bearingless motor B. The bearingless motor B shows a maximum displacement of 23.7 µm, which correlates to a displacement of 7.8% in respect to the radius of the air gap. BM A has an overshoot of 151%, which is similar to what is seen in Fig. 4.5.

For the tuning of the controllers is based on the simulations and has some operational deficiencies, it would be preferable to re-tune it experimentally on the actual prototype system. This re-tuning would likely lead to non-transient responses and more reference-following behavior. Also it would be more preferable to analyze the controller performance against load steps.

5 CONCLUSIONS

This thesis was focused on the creation of a position control system for a bearingless machine. In addition, a linearized simulation model of the system was created. A PID controller was designed using AMB control theory and the linearized simulation model. This way of approach is considered very straightforward, and therefore lacks some controllability in terms of response. The control design that was ended up on will inevitably create some unbalance in the magnetic pull leading to cross effects between the axes.

The simulation model was tested with the designed controllers and on top of that, they were ran on the actual test rig. According to the experimental results, a working control design was achieved. The rotor had a successful lift-up and held its position in the center of the stator fairly well. The simulation results and the experimental results were compared concluding the correctness of the simulation model and the suitability of the control design.

Although the control design was successfully produced, there is still room for improvement. Properties such as position bandwidth and phase margin could be better to ensure the systems stability in different scenarios. In addition, the transient behavior that was found needs to be suppressed to have smoother responses. The overshoot was too high when a displacement was added to the system and it needs to be significantly reduced. For better results, the PID-controllers need to be re-tuned and tested on the actual system to make sure there is no transient behavior. Experimental tuning is required due to the control design's simplicity, for the actual system has nonlinearities and is more complex. The controller's parameters must be selected carefully for the system reacts even to the slightest of changes. This property is most noticeable when derivate gain is modified.

5.1 SUGGESTIONS FOR THE FUTURE WORK

Implementing cross-coupling to the simulation model and the test rig would serve as a good thesis subject. Position bandwidth would also serve as a good subject: what contributes to it and how it manifests itself in a given area.

REFERENCES

Adamczak, S., Stepien, K. & Wrzochal, M., 2017. Comparative study of measurement systems used to evaluate vibrations of rolling bearings. *Procedia Engineering, Proceeding of 12th International Scientific Conference of Young Scientists on Sustainable, Modern and Safe Transport*, Volume 192, pp. 971-975.

Beams, J., 1938. *Suspension of rotatable bodies.* United States, Patent No. 2,256,937.

Bleuler, H., Sandtner, J., Regamey, Y.-J. & Barrot, F., 2005. *Passive Magnetic Bearings for Flywheels.* Lausanne: s.n.

Cansiz, A. & Hull, J. R., 2004. Stable load-carrying and the rotational loss Characteristics of diamagnetic bearings. *IEEE Transactions on Magnetics,* 40(3), pp. 1636-1641.

Chiba, A., Deido, T., Fukao, T. & Rahman, M. A., 1994. An analysis of bearingless ac motors. *IEEE Transactions on Energy Conversion,* 9(1), pp. 61-68.

Chiba, A. et al., 2005. *Magnetic Bearings and Bearingless Drives.* Burlington: Elsevier.

Earnshaw, S., 1842. On the nature of the molecular forces which regulate the constitution of the luminiferous ether. *Trans. Cambridge. Phil. Soc. 7,* pp. 97-112.

Gieras, J., 2010. *Permanent Magnet Motor Technology.* 3rd ed. Boca Raton: CRC Press.

Gräsbeck, K. C., 2018. *Kahden vapausasteen radiaalilaakerijärjestelmän mallinnus ja säätö.* Lappeenranta: Lappeenranta University of Technology.

Habermann, H. & Liard, G. L., 1979. Practical magnetic bearings. *IEEE Spectrum,* Volume 16, pp. 26-30.

Han, H.-S. & Kim, D.-S., 2016. *Magnetic Levitation: Maglev Technology and Applications.* Daejeon: Springer.

Holmes, F. T. & Beams, J. W., 1937. Frictional torque of an axial magnetic suspension. *Nature,* Volume 140, pp. 30-31.

Hynynen, K., 2011. *Broadband excitation in the system identification of active magnetic bearing rotor systems.* Lappeenranta: Lappeenranta University of Technology.

Jiancheng, F., Jinji, S., Yanliang, X. & Xi, W., 2009. A new structure for permanent-magnet-biased axial hybrid magnetic bearings. *IEEE Transactions on magnetics,* 45(12), pp. 5219-5325.

Kandil, M., Dubois, M., Bakay, L. & Trovão, J., 2016. *Experiment on a permanent magnet-biased magnetic bearing with a cascade digital control.* Glasgow, IET.

Kemper, H., 1934. *Schwebebahn mit Räderlosen Fahrzeugen, die an eisernen Fahrschienen mittels magnetischer Felder entlang schwebend geführt werden.*. Germany, Patent No. 643316.

Kurvinen, E., 2016. *Design and simulation of high-speed rotating electrical machinery.* Lappeenranta: Lappeenranta University of Technology.

Lantto, E., 1999. *Robust Control of Magnetic Bearings in Subcritical Machines.* Helsinki: Finnish Academy of Technology.

Larjo, M., 2006. *Aktiivisten magneettilaakereiden tilasäädön mallinnus ja simulointi.* Tampere: Lappeenranta University of Technology.

Majewski, R., Domagalski, R. & Melo, M. M., 2007. Dynamic compensation of dynamic forces in two planes for the rigid rotor. *Journal of Theoretical and Applied Mechanics,* 45(2), pp. 379-403.

Oshima, M. et al., 1996. Characteristics of a permanent magnet type bearingless motor. *IEEE Transactions on Industry Applications,* 32(2), pp. 363-370.

Polajžer, B., 2010. *Magnetic Bearings, Theory and Applications.* Rijeka: SCIYO.

Rai, S., Cavalier, G., Simonelli, J. & Tsao, T.-C., 2016. MIMO Repetitive Control of an Active Magnetic Bearing Spindle. *IFAC-PapersOnLine,* 49(21), pp. 192-199.

Schweitzer, G. & Lange, R., 1976. *Characteristics of a magnetic rotor bearing for active vibration control.* Cambridge, Institution of Mechanical Engineers Conference on Vibrations in Rotating Machinery, pp. 301-306.

Schweitzer, G. et al., 2009. *Magnetic Bearing, Theory, Design, and Application to Rotating Machines.* Berlin: Springer.

Silber, S. et al., 2005. Design aspects of bearingless slice motors. *IEEE Transactions on Mechatronics,* 10(6), pp. 611-617.

University of Surrey, 2010. *The force produced by a magnetic field.* [Online] Available at: http://info.ee.surrey.ac.uk/Workshop/advice/coils/force.html [Accessed 6 7 2018].

Wei, C. & Söffker, D., 2016. Optimization Strategy for PID-Controller Design of AMB Rotor Systems. *IEEE Transactions on Control Systems Technology,* 24(3), pp. 788-803.

Yonnet, J.-P., 1978. Passive magnetic bearings with permanent magnets. *IEEE Transactions on Magnetics,* 14(5), pp. 803-805.

Åström, K. J. & Hägglund, T., 1995. *PID Controllers: Theory, Design and Tuning.* New York: Instrument Society of America.

Åström, K. J. & Murray, R. M., 2008. *Feedback Systems: an introduction for scientists and engineers.* New Jersey: Princeton University Press.

Appendices

Appendix 1: Bearingless prototype machine parameters

BM stands for bearingless motor and FEM for finite element method.

Parameter	**Symbol**	**Value**	**Unit**
Nominal speed	Ω_{nom}	30 000	r/min
Nominal power per motor unit	P_{nom}	5	kW
Rotor mass	m	11.65	kg
Rotor inertia	J	0.232	kgm^2
Resistance, levitation winding	R	0.27	**Ω**
Inductance, levitation winding	L	3.27	mH
BM location	a, b	107.5	mm
Position sensor location	c, d	211	mm
Air gap length	l_{δ}	0.6	mm
Rotor length	l_{r}	480	mm
BM lamination stack length	l_{rl}	61	mm
BM lamination diameter	d_{rl}	68.8	mm
BM stator outer diameter	d_{s}	150	mm
Axial disk thickness	l_{a}	8	mm
Axial disk diameter	d_{a}	112	mm
Rotor shaft diameter	d_{rs}	33	mm
Current stiffness, measured	k_{i}	29	N/A
Position stiffness, measured	k_{s}	672	N/mm
Current stiffness, FEM	$k_{\mathrm{i,FEM}}$	29.6	N/A
Position stiffness, FEM	$k_{\mathrm{s,FEM}}$	618	N/mm